Eur. Phys. J. B **27**, 449–458 (2002)
DOI: 10.1140/epjb/e2002-00177-x

The European Physical Journal B

Optical functions of InGaP/GaAs epitaxial layers from 0.01 to 5.5 eV

R. Ferrini[1], G. Guizzetti[1,a], M. Patrini[1], A. Parisini[2], L. Tarricone[2], and B. Valenti[2]

[1] INFM-Dipartimento di Fisica "A. Volta" dell'Università, Via Bassi 6, 27100 Pavia, Italy
[2] INFM-Dipartimento di Fisica dell'Università, Viale delle Scienze, 43100 Parma, Italy

Received 13 December 2001
Published online 25 June 2002 – © EDP Sciences, Società Italiana di Fisica, Springer-Verlag 2002

Abstract. $In_{0.49}Ga_{0.51}P$ films, both undoped and doped n- and p-type (up to 10^{18} cm^{-3}), were grown lattice matched on GaAs substrates, with different miscut angles, by Metal-Organic Vapour Phase Epitaxy (MOVPE) at different temperatures. The shift of the fundamental gap E_0, caused by "ordering effect" was measured as a function of temperature by photoluminescence. The complex refractive index $\tilde{n} = n + ik$ and the dielectric function $\tilde{\varepsilon} = \varepsilon_1 + i\varepsilon_2$ at room temperature were determined from 0.01 to 5.5 eV by using complementary data from fast-Fourier-transform far-infrared (FFT-FIR), dispersive, and ellipsometric spectroscopies. The effect of the native oxide was accounted for and the self-consistency of the optical functions was checked in the framework of the Kramers-Kronig causality relations. In the restrahlen region the dielectric function was well fitted by classical Lorentz oscillators; in the transparent region below E_0, the refractive index was modelled by a Sellmeier dispersion relation; in the interband region the dielectric function was well reproduced by analytical lineshapes associated to seven critical points. Thus parametrized analytical expressions were obtained for the optical functions all over the spectral range, without discontinuities, to be used in the modelling and characterization of multi-layer structures, also on opaque substrates.

PACS. 78.20.Ci Optical constants (including refractive index, complex dielectric constant, absorption, reflection and transmission coefficients, emissivity) – 78.66.Fd III-V semiconductors – 78.30.Fs III-V and II-VI semiconductors – 78.40.Fy Semiconductors

1 Introduction

$In_xGa_{1-x}P$ mixed crystals have recently gained a considerable technological importance as wide band-gap semiconductors for devices applications [1,2]. In particular $In_{0.484}Ga_{0.516}P$ lattice matched on GaAs has been recognised as an attractive alternative to the AlGaAs/GaAs system to realize Al-free high-quality and high-reliability heterostructure devices [3]. In fact, it has a number of superior features such as: lower oxidation and surface recombination rate; low propagation velocity of dislocations; minor presence of deep level centres (DX-like); strong etch selectivity and a unique opportunity of designing the band gap line-up. Thus a successful fabrication of high performance LED, lasers [4], photonic devices [5], solar cells [6], amplifiers, HBT [7] etc., has been recently reported.

However, depending on growth conditions (*e.g.* V/III ratio, growth temperature, growth rate, doping) and GaAs substrate misorientation, $In_{0.484}Ga_{0.516}P$ shows the formation of domains, with different size and statistical distribution [8], where a spontaneous "ordering" appears in the cationic sublattice: it consists in the alternate sequence of cationic layers along the [111] direction with prevalence of Ga atoms and of In atoms [9]. The strongest fingerprints of "ordering" formation are [10,11] a band gap reduction (BGR) and a splitting of the degenerate valence bands (VBS), caused by the reduced crystal symmetry from T_d (zinc-blende) to the C_{3v}- ($CuPt_B$). Consequently the presence of "ordering" is expected to strongly influence optical and electrical properties of the material, as well as the performances of InGaP-based devices.

The effects of ordering and, at minor extent, of doping on the optical properties of InGaP have been intensively investigated during the last decade. The studies concerned mainly the effects on the energies of phonons, fundamental gap and interband critical points, and reported the measured dielectric functions in the corresponding spectral ranges. However, the differences in the examined samples (growth conditions and doping) and in the experimental techniques make difficult to compare the spectra and merge them to obtain the optical functions on extended spectral regions, which are important for the design and engineering of optoelectronic InGaP-based devices.

More specifically, optical functions at critical points (CPs) have been determined by spectroscopic ellipsometry (SE) on *undoped* epitaxial layers [12–14]; the disorder or doping effects on interband critical points has been

[a] e-mail: guizzetti@fisav.unipv.it

studied by SE [15,16] and compared with first-principles band-structure calculations [10,17]; the refractive index of *undoped* samples has been determined by transmittance or reflectance below and above the fundamental edge [18,19], and the birefringence dispersion below the gap has been measured in (Al)InGaP waveguide structures [20]. IR reflectivity in the reststrahlen region has been measured [21,22] on bulk $\mathrm{In}_x\mathrm{Ga}_{1-x}\mathrm{P}$ in order to determine the dependence of the phonon energies on the concentration x, and on InGaP films (both disordered and ordered) using polarized light to evidence anisotropy of the dielectric function [23]. Low-temperature photoluminescence (PL) and photoluminescence excitation (PLE) spectroscopy have been used to investigate the role of growth parameters and substrate misorientation on the ordering, determined through the band-gap reduction and valence-band splitting of *undoped* InGaP [24].

For all the aforementioned reasons, the aim of this paper is to accurately determine the complex refractive index $\tilde{n}(\nu) = n(\nu) + \mathrm{i}\,k(\nu)$ and the dielectric function $\tilde{\varepsilon}(\nu) = \varepsilon_1(\nu) + \mathrm{i}\,\varepsilon_2(\nu) = \tilde{n}^2(\nu)$ of $\mathrm{In}_{0.49}\mathrm{Ga}_{0.51}\mathrm{P}$ films over a wide spectral range (0.01–5.5 eV), for different miscut angles of the GaAs substrate, doping and growth conditions. Particular attention has been paid to the medium- and near-infrared (MIR and NIR) regions, where InGaP-based optical devices mainly work, and to the shift of the fundamental optical gap E_0, induced by ordering.

$\mathrm{In}_{0.49}\mathrm{Ga}_{0.51}\mathrm{P/GaAs}$ samples were grown by Metal-Organic Vapour Phase Epitaxy (MOVPE) and well-characterized to assure good structural, compositional and optical quality. Fitting of the experimental spectra with analytical models was performed to obtain a parametrization, which allows $\tilde{\varepsilon}$ and n to be calculated for any photon energy on a wide spectral range. In particular Lorentz oscillators in the restrahlen region, the Sellmeier dispersion relation in the subgap transparency region and two parametric semiconductor models for the CPs in the inter-band region have been adopted. The derived parameters and the database for n and k can play an important role not only in the analysis and interpretation of the experimental spectra, but also in optoelectronic applications and diagnostics, *e.g.* to characterize composition, free-carrier concentration, homogeneity and thickness of InGaP films in multilayer structures.

2 Experimental details and data reduction

Two series of $\mathrm{In}_{0.49}\mathrm{Ga}_{0.51}\mathrm{P/GaAs}$ films of different doping density and conductivity were prepared by Metal-Organic Vapour Phase Epitaxy (MOVPE) through different apparatus: the samples of the EPI series were grown, at a temperature $T_g = 700$ °C, according to the request of the purchaser by the Epitaxial Products International; the samples of the BTS series were grown at the Institute of Electronic Engineering of the Academy of Science of Bratislava ($T_g = 640$ °C); the GaAs substrates were oriented along the (100) direction, either 2° or 10° miscut toward the [110] direction. As concerns the composition inhomogeneity, related to the gas flux direction into the reactor chamber, it is important to remark that samples of EPI and BTS series were both grown in AIXTRON 200 plants, supplied (EPI) and not supplied (BTS) of a "gas foil rotation" (susceptor rotation system). According to the results reported in reference [25], the growth of undoped $\mathrm{In}_{0.5}\mathrm{Ga}_{0.5}\mathrm{P}$ layers at $T_g = 640$ °C on a GaAs substrate 2° miscut toward the [110] direction should give the maximum ordering, that is the maximum BGR. The value of the order parameter η (with $0 \le \eta \le 1$) of the samples was estimated from the measured changes in the fundamental band gap, as explained below. In Table 1 the sample parameters are summarised. Carrier densities were determined at room temperature by the suppliers, through either Hall or C-V profile measurements. The compositional homogeneity was carefully measured by High Resolution X-ray Diffraction. In the BTS samples the mean lattice mismatch $[\Delta a/a]^{\perp}$ averaged over the film thickness was -1.74×10^{-3}, corresponding to a mean composition $x = 0.471$ [26]. As a consequence, the critical misfit strain is exceeded and the layers get plastically relaxed giving rise to misfit dislocations at the layer/substrate interface. In the case of EPI samples the measured In content was $x = 0.481$. As it appears in Table 1, nominal film thicknesses were in the range 1–3.5 μm; the actual values were determined from the interference fringes in the subgap region of the reflectance spectra (see below).

Table 1. Specifications of the InGaP layers on GaAs substrate used in this work.

Sample	Miscut Angle	T_g (°C)	Nominal Thickness (μm)	Doping level (10^{16} cm^{-3})
EPI61	10°	700	3.15	u/d
EPI62	2°	700	3.15	$n < 2.1\text{e-}2$
EPI71	10°	700	3.15	$n = 16$
EPI72	2°	700	3.15	$n = 10$
BTS142	2°	640	1.5	$n = 4.2$
BTS143	2°	640	1.5	$n = 57$
BTS144	2°	640	1	$p = 45$
BTS145	2°	640	1	$n = 100$

Optical spectroscopy measurements were performed on all the samples. Room temperature reflectance (R) at near-normal incidence was measured in the wavenumber range 100–5000 cm^{-1} (0.012–0.6 eV) with a Bruker IFS 113v spectrometer, at a spectral resolution of 0.5 cm^{-1} from 100 to 600 cm^{-1} (FIR) and 4 cm^{-1} from 600 to 5000 cm^{-1} (MIR). A LHe cooled Si-bolometer and a deuterated triglycerine sulphite (DTGS) pyroelectric were used as detectors in FIR and MIR, respectively. The accuracy in the wavenumber calibration was 0.01 cm^{-1} and the absolute reflectance was accurate to $\pm\,0.005$. In the 0.4–6 eV photon energy range (NIR-UV) R was measured using a Cary 5E automatic spectrophotometer, with a photometric accuracy of 0.5% and spectral resolution better than 0.5%. An Al mirror and an Au mirror covered with MgF_2 film, whose absolute reflectivity was directly measured, were used as references for R in the NIR-UV

and MIR-FIR, respectively. The spectra from different apparatus merge one into the other, within the experimental uncertainty.

The ellipsometric functions $\tan\psi$ and $\cos\Delta$ (with $\tilde{\rho} = \tan\psi\exp(\mathrm{i}\Delta)$, where $\tilde{\rho}$ is the complex ratio of the parallel to perpendicular polarization reflection coefficients) were measured between 1.4 and 5 eV by an automatic ellipsometer Sopra mod. MOSS ES4G. The system uses a 75W xenon lamp, a rotating polarizer, an auto-tracking analyzer, a double monochromator and a single-photon-counting photomultiplier detector system. $\tan\psi$ and $\cos\Delta$ were measured with a typical standard deviation less than 0.005, with a mesh of 10 meV and a spectral resolution of 1 meV, at two angles of incidence ($\phi = 75 \pm 0.05°$ and $70 \pm 0.05°$), close to the Brewster angle for optimum sensitivity.

The pseudodielectric function $\langle\tilde{\varepsilon}\rangle = \langle\varepsilon_1\rangle + \mathrm{i}\langle\varepsilon_2\rangle$ of the InGaP films was obtained by the measured complex reflectance ratio $\tilde{\rho} = \tan\psi\exp(\mathrm{i}\Delta)$ in the two-phase model:

$$\langle\tilde{\varepsilon}\rangle = \varepsilon_a\left(\sin^2\phi + \sin^2\phi\,\tan^2\phi\left(\frac{1-\tilde{\rho}}{1+\tilde{\rho}}\right)^2\right) \qquad (1)$$

where ε_a is the dielectric function of the ambient. The comparison with previous spectra measured by SE on InGaP/GaAs samples [13] showed that our $\langle\varepsilon_1\rangle$ and $\langle\varepsilon_2\rangle$ spectra, as expected, were affected by a surface overlayer. Therefore, to mathematically remove the effects of the native oxide on $\langle\tilde{\varepsilon}\rangle$ we adopted a three-phase model (ambient-oxide-InGaP) in the inversion of the SE spectra in the 4–5 eV range, where the InGaP is strongly absorbing. The dielectric function $\tilde{\varepsilon}_{ox}$ of the InGaP-oxide was obtained as a 50% average of the $\tilde{\varepsilon}_{ox}$ of InO_3- and GaO_3 native oxides, taken from literature [27], and its effective thickness was estimated to be $d_{ox} = 3.2 \pm 0.3$ nm.

The consistency of ε_1 and ε_2 (and of n and k) directly obtained from SE and from R outside the ellipsometric range, was checked through the Kramers-Kronig (K-K) causality relations by using the method described in reference [28], which is not sensitive to overlayers such as oxides or microscopic roughness, but is sensitive to experimental artefacts. To perform the K-K transform we extrapolated the R spectrum beyond 6 eV with a two-parameter tail, constructed to fit, at two different energies, the values of n and k as obtained by SE. The normalized difference $(\varepsilon_1 - \varepsilon_{1\mathrm{KK}})/\varepsilon_{2pk}$, where $\varepsilon_{1\mathrm{KK}}$ is the KK transform of ε_2 and ε_{2pk} is the peak value of ε_2, lays within $\pm 0.5\%$, according to the self-consistency values quoted in reference [28].

Photoluminescence measurements from 1.7 to 2.1 eV were performed at different temperatures in the range 10–300 K. The exciting source was an Argon laser ($\lambda = 514.5$ nm); the power density of the incident light on the sample was about 0.6 W/cm^2 (power on the sample of ∼5 mW). The light emitted by the samples was then analysed by a 0.5 m Jobin Yvon-Spex HR 460 single monochromator and detected by a cooled PbS detector using a conventional lock-in technique. The spectral resolution of the optical system was 1 meV. At low temperature the PL spectra were also taken at different power values in the range 0.01 mW to 100 mW.

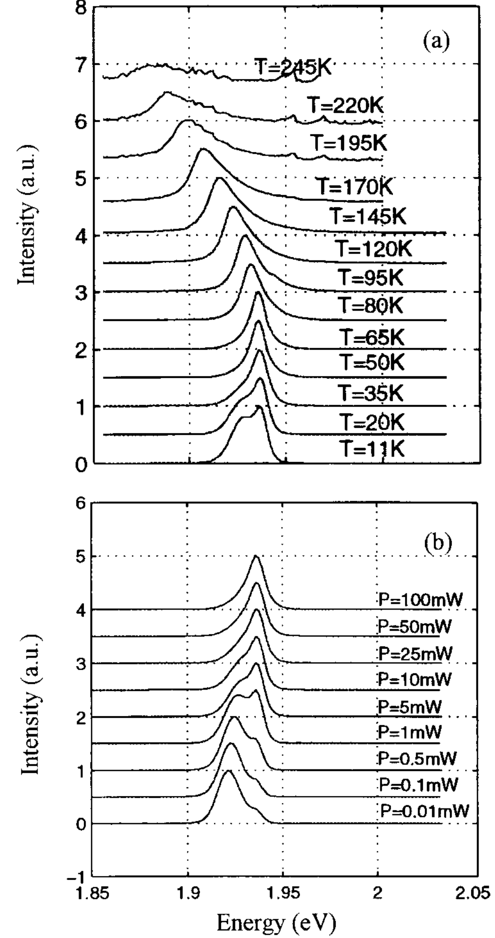

Fig. 1. Photoluminescence spectra of sample EPI62: (a) at different temperatures, with light power on the sample $P = 5$ mW and (b) for different power values at $T = 11$ K.

3 Results and discussion

3.1 Ordering effects on E_0 fundamental gap

As pointed out before, peculiar growth conditions and GaAs substrate misorientation induce the formation of domains where a spontaneous "ordering" appears and the crystal symmetry lowers: their effects on the fundamental gap E_0 in our samples have been analysed by photoluminescence [8,24].

As a general feature, PL spectra measured on the BTS samples display a higher broadening of the structures with respect to the EPI series. This fact is consistent with the appreciable compositional inhomogeneity, determined by the X-ray investigation [22], which in addition causes the rapid quenching of the PL efficiency for increasing temperatures, due to the activation of non-radiative recombination processes. In Figure 1a typical PL spectra relative to the EPI62 sample are reported, as a function of temperature T. All the spectra beside the band-to-band transition structure E_0, which red-shifts with increasing T owing to the band gap shrinkage, display a anomalous emission band at lower energies (LE), which blue-shifts

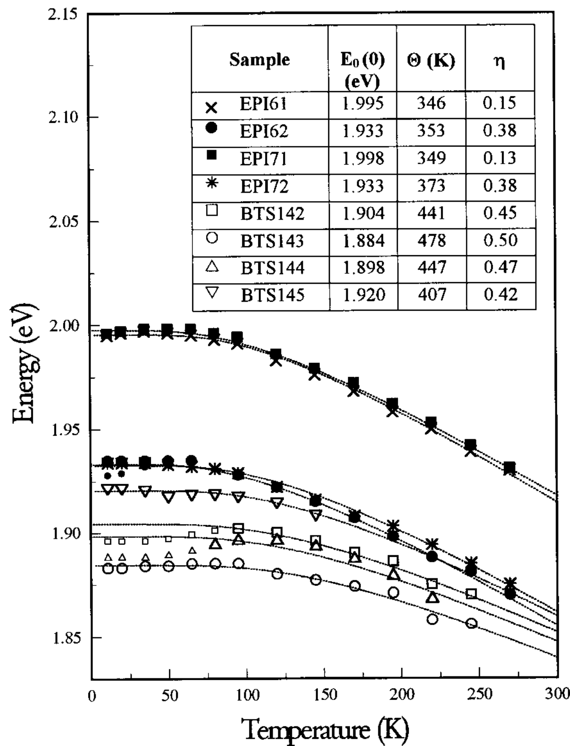

Fig. 2. Temperature dependence of the main PL peaks for all the samples: either the LE or the E_0 peaks are reported for the same sample, using the same symbols with different size (smaller or bigger, respectively). In the case of sample EPI62 both emissions are reported, the corresponding PL peaks being well resolved. The best fits of $E_0(T)$ to the analytical lineshape (Eq. (2)) are shown (dotted lines), and their free-parameter values are reported in the inset, together with the order parameter η.

with T. In the EPI62 sample the two peaks are well resolved at low temperatures; however the convolution of E_0 and LE bands gives a anomalous s-shaped behaviour of the PL spectra as a function of temperature. A monotonic displacement toward higher energies of the LE emission is observed as the laser power on the sample increases (Fig. 1b): this behaviour is recognised as a fingerprint of the presence of ordering. In the case of disordered InGaP samples only an increasing intensity of the PL peak is observed for increasing laser power density, without any energy shift.

The appearing in some samples (EPI62, BTS142 and BTS144) of this anomalous band at energies lower than E_0 reveals a significant presence of "anti-phase boundaries" [29–32] between regions characterised by a some degree of CuPt_B order [24], with the prevalence, in the present cases, of small size ordered domains with a large statistical distribution of the domain size [8,26]. However, the lack of the LE emission in the other samples does not exclude the presence of "ordering", whose main effect is a reduction of the fundamental band gap and a splitting of the valence band at the Γ point [9,11], as a consequence of the crystal symmetry lowering.

The temperature dependence of the peak energy of the main PL emission bands is reported in Figure 2 for all the samples: E_0 transition and anomalous emission band are distinguished through symbols of equal shape and different dimensions for each sample. The energies were obtained by fitting the PL spectra using a Gaussian profile, through the deconvolution of the HE and LE contributions whenever appropriate. The resulting E_0 energies were fitted to the empirical formula of Lautenschlager, Allen and Cardona [33],

$$E_0(T) = E_0(0) - \frac{K}{\exp(\Theta/T) - 1}\,. \tag{2}$$

$E_0(0)$, K and Θ are phenomenological free parameters; in particular Θ should be related to an averaged phonon temperature. All the data were fitted simultaneously by forcing the K free parameter to be the same for all curves: the accuracy was $\chi^2 \sim 3\times10^{-6}$ and the confidence limits of the parameters were about 0.1% for $E_0(0)$, 10–20% for K and 10–20% for Θ. This constraint allows us: i) to avoid a meaningless scattering of the correlated Θ and K parameters; ii) to better evidence differences in the temperature dependence of the curves, without appreciably limiting the fit accuracy and influencing $E_0(0)$. The lines in Figure 2 give the results of the fit, with $K = 0.175$, whereas the values of the free parameters $E_0(0)$ and Θ, as well as the order parameter η, are collected in the inset.

The degree of order of the samples was estimated using the equation [10]

$$E_g^{\eta} = E_g^{\eta=0} - \Delta E_g^{\eta=1}\,\eta^2 \tag{3}$$

where E_g^{η} is the measured gap ($E_0(0)$ in our case); $E_g^{\eta=0}$ and $E_g^{\eta=1}$ are the gaps of the perfectly random and the perfectly ordered alloy, respectively; and $\Delta E_g^{\eta=1} \equiv E_g^{\eta=0} - E_g^{\eta=1}$. The values $E_g^{\eta=0} = 2.007$ eV and $\Delta E_g^{\eta=1} = 0.49$ eV are taken from reference [11].

Only the EPI61 and EPI71 samples resulted quasi completely disordered, whereas a relevant degree of order resulted for the BTS142, BTS144 and BTS143 samples. As expected, the 2° miscut angle produces higher ordering with respect to the 10° miscut (see the undoped samples EPI 61 and EPI62 or the doped ones EPI71 and EPI72). Moreover, at the same miscut angle and doping, the disorder increases with increasing the growth temperature (see samples EPI72 and BTS142).

Concerning the doping effects, in a semiconductor the optical transitions near E_0 are generally influenced by doping and structural disorder (band tails, degeneration, many body effects): in n-type InGaP the critical density for the appearing of the Burstein-Moss effect is of a few 10^{16} cm^{-3}. On the other hand it has been experimentally shown that the increasing doping reduces the ordering effects [34], so that the measured E_0 is the result of the two competitive effects. In the case of samples BTS143 and BTS144 the many-body effect related to the increasing doping prevails causing a gap-shrinkage with respect to the less doped sample (BTS142), whereas the BTS145 sample exhibits the highest E_0 among the BTS samples, suggesting the reduced ordering effect to prevail.

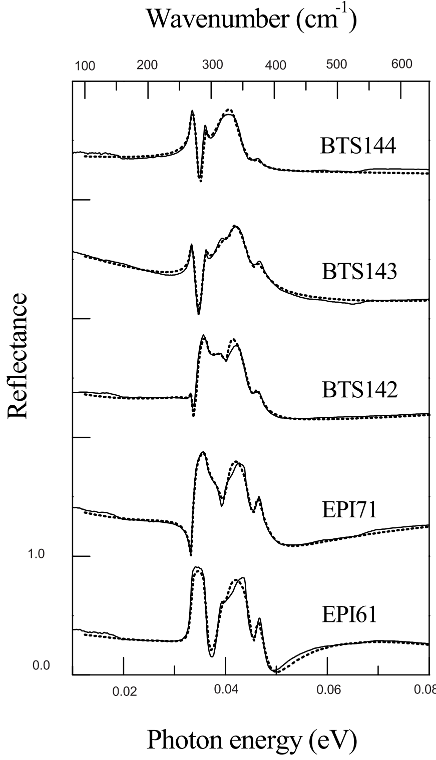

Fig. 3. FIR reflectance spectra (full lines) of InGaP films on GaAs with different thickness and doping and their best-fits (dotted lines). Each spectrum is displaced vertically by 1.0 to facilitate viewing.

From the comparison of the two series of samples shown in Figure 2 a stronger temperature dependence is observable for the less "ordered" samples (EPI series) with respect to the BTS samples, resulting in a lower value of the Θ parameter. A more detailed discussion on these results is reported in reference [25].

3.2 Restrahlen region

The FIR reflectance spectra of five samples from 100 to 650 cm^{-1} are shown in Figure 3 (full line). All spectra display two higher-energy bands, one at $\sim$330 cm^{-1} and the other one at $\sim$370 cm^{-1}, which are typical of two-mode III-V alloys and are due to IR-active transverse-optical (TO) phonons, with energy ν_{TO}: they can be characterized as InP-like and GaP-like, respectively, because of their energy relationship to the restrahlen bands of InP (ν_{TO} = 303.7 cm^{-1}) and GaP (ν_{TO} = 367 cm^{-1}). The peak at 270 cm^{-1} is due to the TO-phonon of the GaAs substrate, while the lower-energy tail, increasing with doping, represents the free-carrier response.

Amplitude, position and shape of the FIR bands strongly depend on the alloy composition as well as on the layer thickness and doping. The shoulders appearing between the GaAs and InP-like peaks are due to interference effects, caused by multireflections at the interfaces between the InGaP layer and the air or the substrate. In the transparency regions ($\nu < 250$ cm^{-1} and $\nu > 450$ cm^{-1}), instead, some little oscillations in R are due to two-phonon absorption; the little steps at $\sim$540 cm^{-1} and $\sim$150 cm^{-1} are due to contributions to R from the back-surface of GaAs substrate, which is difficult to evaluate because this surface was not optically polished.

In order to obtain the optical functions, the experimental spectra were fitted with the R analytical expression for a three-phase system (air-InGaP layer-GaAs substrate), assuming the InGaP effective thickness deduced by the interference fringes in the MIR region (see below). The complex dielectric function $\tilde{\varepsilon}(\nu)$ of InGaP was constructed as a superposition of three damped harmonic oscillators corresponding to the InP- and GaP-like phonon modes and to the free carriers, respectively. Hence:

$$\tilde{\varepsilon}(\nu) = \varepsilon_{\infty} + \sum_{j=1}^{2} \frac{S_j^2}{\nu_{\mathrm{TO},j}^2 - \nu^2 + \mathrm{i}\,\Gamma_j \nu} - \frac{\nu_p^2}{\nu^2 + \mathrm{i}\,\gamma\,\nu} \quad (4)$$

where ε_{∞}, $\nu_{\mathrm{TO},j}$, S_j, Γ_j, ν_p, γ (which are also the free-parameters of the fit) represent, in order, the high-frequency dielectric constant, the frequency, the oscillator strength and the phenomenological damping of the TO phonons, the plasma frequency and the damping of the free carriers. The values $\varepsilon_{\infty} = 11.1$, $\nu_{\mathrm{TO}} = 268.7$ cm^{-1}, $S = 380$ cm^{-1}, $\Gamma = 2.4$ cm^{-1} for the GaAs substrate were fixed and kept from literature [35].

We considered all the samples to be isotropic: this assumption can appear correct for highly disordered phase, which has the cubic zincblende structure, but not for the ordered one, which has trigonal symmetry; in this case the dielectric function should be a tensor, with component parallel and perpendicular to the ordering axis, as discussed in detail in reference [23]. In the same paper, however, off-normal incidence reflectance, measured with polarized light on *undoped* samples both ordered and disordered, showed that GaP-like structures is not affected by ordering; instead, a little structure in R, centered at 355 cm^{-1}, appears in p-polarized spectra as the order parameter increases, due to the splitting of the LO InP-like phonons. In our R spectra, taken with unpolarized light at near-normal incidence, this weak structure was not detectable.

The least-squares fit, giving a standard deviation $\sigma \leq 2 \times 10^{-2}$ for all the spectra, was carried out using the CERN library MINUIT program, based on the Metropolis algorithm. Regarding the fit quality, we note that the biggest discrepancy between experimental and fitted spectra (full and dotted lines, respectively, in Fig. 3) concerns the peak of the structure at $\sim$330 cm^{-1}. This discrepancy, which was also present in the results of reference [23], can be ascribed to the assumption of abrupt interface between film and substrate, while a transition region, caused by interdiffusion, is probably present. Moreover our model does not include two-phonon contribution to $\tilde{\varepsilon}(\nu)$ nor the GaAs back-surface contribution to R, giving the aforementioned features in the experimental spectra.

The best-fit parameters are reported in Table 2 and deserve some comment:

a) $\varepsilon_{\infty} = 9.4 \pm 0.04$ value, lying between the extreme values of 9.61 for InP and 9.09 for GaP [35], is consistent

Table 2. Harmonic oscillator parameters from the best fit to the reflectance spectra of InGaP layers on GaAs in the far infrared spectral region and Sellmeier parameters from the fit to the refractive index n below the fundamental energy gap E_0.

Sample			InP-like mode			GaP-like mode			Free-carriers		Sellmeier parameters		
	N (10^{16}cm^{-3})	d (μm)	ν_{TO} [cm^{-1}]	S [cm^{-1}]	Γ [cm^{-1}]	ν_{TO} [cm^{-1}]	S [cm^{-1}]	Γ [cm^{-1}]	ν_p [cm^{-1}]	γ [cm^{-1}]	A	B	C [μm]
EPI 61	u/d	3.23	329.1	526.2	9.92	371	113.5	8.1	235.2	20	6.058	3.27	0.459
EPI 71	$n-16$	2.13	329.9	523.5	10.02	370.6	124.1	8.16	316.2	73.6	6.061	3.29	0.454
BTS 142	$n-4.2$	1.5	328.1	526.5	7.75	370.3	101.3	9.77	330	58.1	6.074	3.21	0.460
BTS 143	$n-57$	1.32	331.9	499.7	9.58	371.6	121.2	12.35	706.8	93.7	5.737	3.55	0.446
BTS 144	$p-45$	0.816	327.2	524.4	8.78	371.1	102.4	13.5	472.3	182	5.676	3.65	0.452

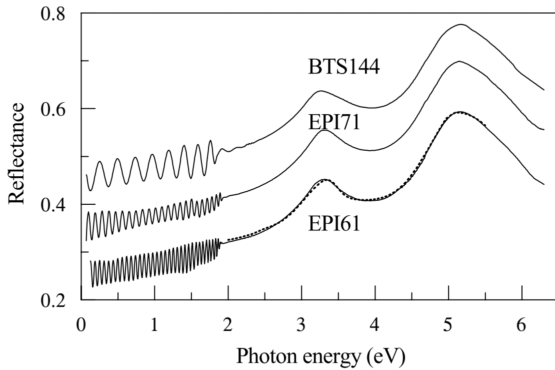

Fig. 4. NIR-UV reflectance spectra of InGaP samples EPI61, EPI71 and BTS144 (full lines). Each spectrum is displaced vertically by 0.1 to facilitate viewing. For sample EPI61 the best-fit to PSM model is also reported (dotted line).

with the dielectric response at higher frequencies, and is in good agreement with the value of 9.43 ± 0.02 quoted in reference [13]. For undoped $\text{In}_{0.49}\text{Ga}_{0.51}\text{P}$ (sample EPI61) ε_∞, $\nu_{\text{TO},j}$, S_j, Γ_j values, inserted in equation (2) for $\nu = 0$, give a static dielectric constant $\varepsilon_0 = 12.05$.

b) ν_{TO} values agree within 2% with $\nu_{\text{TO}} = 333$ cm^{-1} and $\nu_{\text{TO}} = 370$ cm^{-1} for InP-like and GaP-like, respectively, quoted in reference [36] collecting results from different works, and should be compared with those corresponding of InP ($\nu_{\text{TO}} = 303.7$ cm^{-1}) and GaP ($\nu_{\text{TO}} = 363.4$ cm^{-1}) [35]. In particular they only differ by ± 1 cm^{-1} from the values obtained in reference [23] by fitting R spectra with a dielectric tensor. Unfortunately in this work the oscillator strength and the damping values are not given, so that a deeper comparison is not possible. ν_{TO} values change little with doping, indicating that at the actual free-carrier concentrations the electron-phonon interaction is rather weak.

c) Γ_j and γ values, instead, strongly increase with doping, both for increasing disorder and electron scattering from ionised impurities.

3.3 Subgap transparency region and interband region

In Figure 4 the R spectra for three typical samples (EPI61, EPI71 and BTS44, *i.e.* undoped, n- and p-type doped, respectively) are reported for photon energies from 0.07 to 6 eV. The spectra of the other samples, displaying the same behaviour, are omitted. Due to multiple internal reflections within the film, extending down to the restrahlen region, regular interference oscillations in R spectra start up just below the fundamental absorption edge E_0 at ~1.9 eV. The amplitude and period of the fringes change from one sample to the other, due to the different effective thickness and refractive index. The first interference fringe, in correspondence of E_0, is red-shifted in the samples with a miscut angle of 10° with respect to those with a miscut angle of 2°.

All the spectra display two main structures, E_1 peaked at ~3.4 eV and E_2 at ~5.2 eV, typical of the III-V zincblende semiconductors. They originate from direct optical transitions around the interband critical points in the Brillouin zone (BZ): the E_1 transitions take place along the Λ direction, while E_2 consists of several CP contributions arising mainly from transitions along the Σ line and near the X-point of the BZ. The energy position of these peaks is intermediate between that of the corresponding peaks of InP ($E_1 \approx 3.2$ eV and $E_2 \approx 5.1$ eV) and GaP ($E_1 \approx 3.7$ eV and $E_2 \approx 5.4$ eV) [28]. Shape, intensity and peak positions are practically constant for all samples, except a little red-shift of E_1, more evident in the spectra deduced from SE, increasing with ordering, as discussed in reference [16].

In Figure 5 the ellipsometric spectra $\tan\psi$ and $\cos\Delta$ of a typical sample (EPI61) from 1.4 to 5 eV and at two incidence angles (70° and 75°) are reported (full lines). In order to derive the optical functions from the experimental R and SE spectra and fit them with analytical expressions we proceeded as follows.

At first we determine $n(\nu)$ in the transparency region of InGaP ($k(\nu) = 0$ from ~0.05 to 1.8 eV) and the actual thickness d by fitting the interference fringes in R, through the well-known relations for the reflectance of a multilayer [37] and the Sellmeier dispersion relation:

$$n^2 = A + B\frac{\lambda^2}{\lambda^2 - C^2} \tag{5}$$

where A, B and C are variable fit parameters. Then we use the value of d and d_{ox}, to invert $\tan\psi$ and $\cos\Delta$ with a four-phase model (ambient-oxide-film- GaAs substrate), thus obtaining $\tilde{\varepsilon}(\nu)$, $n(\nu)$, and $k(\nu)$, which merge without discontinuities in the restrahlen-region spectra. The resulting ε_1 and ε_2 spectra, except for photon energies near

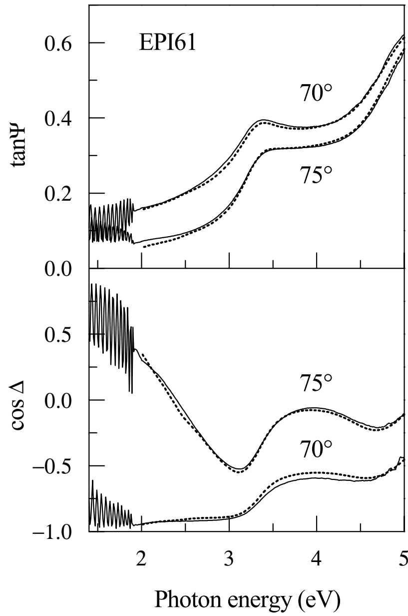

Fig. 5. Ellipsometric spectra of sample EPI61 at two angles of incidence 70° and 75°. The best-fit to PSM model is also reported (dotted line).

the band gap, are practically the same for all samples and well agree (within 5%) on the overall SE range with those obtained previously on ordered [13] and disordered [14] undoped samples, which accounted for the surface oxide as well. Our values of ε_2 at E_1 and E_2 peaks instead are systematically higher (the difference increasing with photon energy, up to 30% at E_2) than those reported in reference [12], where the oxide effect was not removed from the pseudodielectric function. Our results support the conclusion that oxide effects are very important and that the observed miscut-angle dependence of ε_2 in reference [12] results mainly from the difference in the surface roughness and oxide thickness.

The next step was to fit simultaneously the spectra from 0.08 to 6 eV of R at normal incidence and of $\tan\psi$ and $\cos\Delta$ at two different incidence angles, using the software package by Woollam Inc., based on $\tilde{\varepsilon}(\nu)$ parametric semiconductor model (PSM) of C.C. Kim *et al.* [38], which has been successfully applied to AlGaAs alloys [39]. This model is more generally valid than other models, which are purely phenomenological (like the harmonic-oscillator one) or based on parabolic-band approximation (Critical-Point Parabolic Band, CPPB model): it is applicable both below and above the fundamental gap E_0, giving the correct analytic structure of the joint density of states at each interband critical point (E_0 included). Moreover it satisfies the Kramers-Kronig relations and combines Lorentzian and Gaussian broadening. In our case seven critical points are sufficient to reproduce accurately the interband dielectric function, which well fit all the experimental different spectra.

A typical best-fit (sample EPI61) is shown (dotted line) in Figure 4 for R and in Figure 5 for SE spectra, while in Figure 6 the detailed fit for the interference fringes

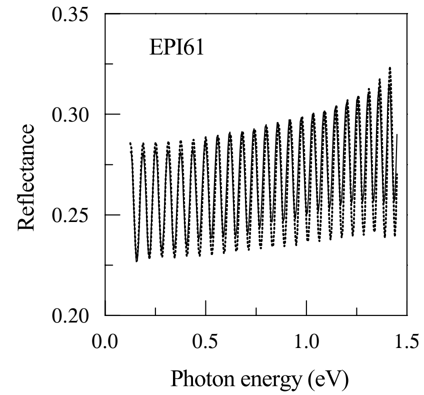

Fig. 6. Reflectance interference fringes in the subgap region for InGaP sample EPI61 on GaAs substrate (full line) and their best fit (dotted line).

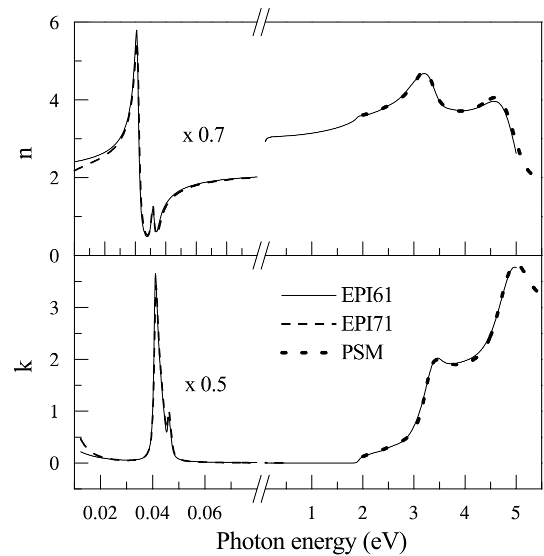

Fig. 7. Refractive index n and extinction coefficient k from FIR to VUV region for the samples EPI61 (full line) and EPI71 (dashed line). Interband optical functions for EPI61 sample as derived from PSM are also reported (dotted lines).

is reported. We note that the resulting n spectra from Sellmeier model and PSM model are quasi coincident in the 0.05–1.8 eV energy range. Obviously, better agreement between experiment and analytical model should be obtained by separately fitting each R and SE spectrum, but in this case the derived $\tilde{\varepsilon}(\nu)$ spectra should not coincide. The simultaneous fit is the best compromise for fitting spectra from different techniques and different angles of incidence. In addition we note that, apart from the period, the amplitude of the interference fringes is hardly reproduced when assuming abrupt, plane and parallel interfaces, as already mentioned concerning the FIR spectra.

3.4 Overall n(ν) and k(ν) spectra

In Figure 7 we report the refractive index (n) and the extinction coefficient (k) spectra of EPI61 and EPI71 samples in the region from 0.01 to 5.5 eV. As expected, the

major differences between the two samples (and other samples) are in the FIR region, due to the free carrier contribution, and around the absorption edge. Above E_0 the two spectra are practically coincident (and not distinguishable in the figure). From 0.01 to 0.08 eV the spectra were obtained from Drude-Lorentz oscillators (Eq. (4)) using the fitted parameter values reported in Table 2. From 0.05 to 1.9 eV n spectra follow Sellmeier dispersion (Eq. (5)) with the parameters A, B, C reported in Table 2 and well connect to the FIR spectra. From 1.9 to 5 eV n and k spectra were obtained from the inversion of SE spectra in the four-phase model. The corresponding n, k, ε_1 and ε_2 values for the EPI61 sample are reported in Table 3. n and k (dotted line) as obtained from the parametric semiconductor model are also shown in Figure 7.

Beyond the PSM model, we employed the well-known Adachi's critical-point model (MDF) [40] for the parametrization of the interband complex dielectric function. This model augments a CPPB model with a phenomenological contribution at higher energies. Its main advantage is that it has already been applied to a number of compound semiconductors [40], and in particular to InGaP [14]. Moreover, this model has a reduced number of parameters with respect to the PSM; in Table 4 we report the complete set of parameters, which we obtained for the EPI61 sample using the Adachi's equations as reported in reference [14]. We note that the MDF fit to the experimental dielectric function is not as good as the PSM one, above all near the E_1 and E_2 peaks and at the absorption edge.

For more clarity we report in Figure 8 the expanded spectra of n and k for all samples around the fundamental gap E_0, *i.e.* the region of highest interest for applications and multilayer diagnostic. We note that, apart from the shift of the absorption edge E_0, no differences are detected within the experimental uncertainty for samples with a different degree of ordering or doping. In reference [20] a difference between the ordinary refractive index n_o and the extraordinary one n_e (parallel and perpendicular to the ordering planes, respectively) has been measured in the 1.5–1.8 eV range on ordered InGaP in waveguide structures. The value of this difference, less than 0.02, is beyond the attainable precision of R, T or SE techniques.

4 Conclusions

Two series of $In_{0.49}Ga_{0.51}P$ thin layers were grown by MOVPE, using two different apparatus and temperatures, on (100) GaAs substrates with different miscut angles (2° and 10°) toward the [110] direction. The films were both undoped and doped n- and p-type (up to 10^{18} cm^{-3}).

The photoluminescence spectra around the fundamental edge gave evidence of the E_0 energy displacements associated to different factors: short-range ordering in the cation sublattice, doping level and structural disorder. In particular the ordering parameter η was obtained from E_0 for each sample. Moreover, the dependence of E_0 on T was determined and well fitted by an empirical formula.

Table 3. Refractive index n, extinction coefficient k, real and imaginary part of the dielectric function ε of the undoped and highly disordered InGaP layer on GaAs substrate (sample EPI61).

Energy (eV)	n	k	ε_1	ε_2
1.9	3.588	0.077	12.869	0.554
2.0	3.612	0.123	13.033	0.889
2.1	3.643	0.164	13.244	1.197
2.2	3.680	0.198	13.506	1.461
2.3	3.727	0.228	13.841	1.701
2.4	3.788	0.261	14.280	1.978
2.5	3.853	0.306	14.755	2.360
2.6	3.918	0.351	15.229	2.748
2.7	3.999	0.391	15.842	3.130
2.8	4.107	0.442	16.672	3.632
2.9	4.244	0.518	17.744	4.395
3.0	4.416	0.639	19.096	5.646
3.1	4.604	0.863	20.450	7.949
3.2	4.677	1.260	20.285	11.789
3.3	4.574	1.716	17.977	15.701
3.4	4.263	1.964	14.316	16.749
3.5	3.982	1.980	11.937	15.766
3.6	3.836	1.938	10.954	14.869
3.7	3.760	1.910	10.487	14.364
3.8	3.723	1.898	10.257	14.128
3.9	3.713	1.901	10.168	14.116
4.0	3.722	1.922	10.163	14.305
4.2	3.750	1.959	10.222	14.690
4.2	3.795	2.017	10.337	15.308
4.3	3.861	2.105	10.482	16.253
4.4	3.945	2.241	10.540	17.679
4.5	4.027	2.451	10.206	19.741
4.6	4.061	2.753	8.913	22.362
4.7	3.981	3.126	6.074	24.892
4.8	3.741	3.493	1.797	26.138
4.9	3.352	3.755	−2.864	25.173
5.0	2.914	3.834	−6.203	22.344
5.1	2.528	3.765	−7.788	19.036
5.2	2.255	3.604	−7.908	16.253
5.3	2.098	3.439	−7.429	14.431
5.4	2.009	3.317	−6.969	13.325
5.5	1.943	3.236	−6.697	12.579

Table 4. Free-parameter values of the best-fit of the InGaP interband complex dielectric function (sample EPI61) to the Adachi MDF model.

Parameter	Value
ε_∞	0.30
E_0 (eV)	1.91
A_0 (eV$^{1.5}$)	7.48
Γ_0 (eV)	0.08
E_1 (eV)	3.30
A_1	5.72
Γ_1 (eV)	0.418
A_{1x} (eV)	1.73
Γ_{1x} (eV)	0.206
S_{1x} (eV^{-2})	0.48
P_{1x}	−0.44
E_2 (eV)	4.88
A_2	2.64
Γ_2 (eV)	0.734
S_2 (eV^{-2})	0.7
P_2	0.16

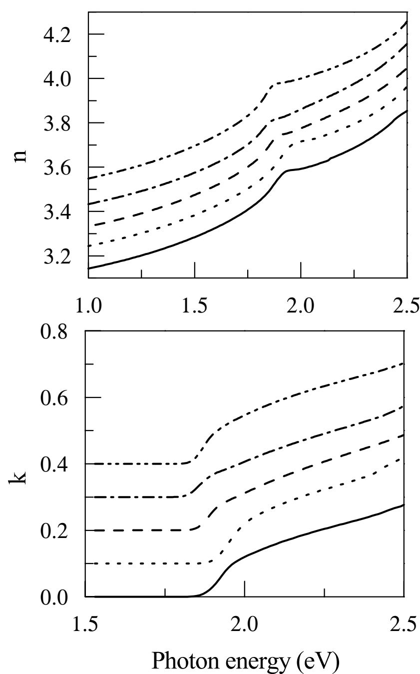

Fig. 8. Refractive index n and extinction coefficient k in the fundamental gap spectral region for samples (from bottom to top) EPI61, EPI71, BTS142, BTS143 and BTS144. Each spectrum is shifted vertically by 0.1 to facilitate viewing.

The real and imaginary parts of the complex dielectric function, the refractive index and the extinction coefficient were determined from 0.01 to 5.5 eV through normal incidence reflectance and spectroscopic ellipsometry. Their consistency was checked with the Kramers-Kronig causality relations, and the effect of the native oxide was accounted for.

The optical functions were modelled with the following analytical lineshapes: Drude-Lorentz oscillators in the restrahlen region, the Sellmeier relationship below E_0 and a complete critical-point model (which goes beyond the parabolic-band and the Lorentzian broadening approximations) in the interband region. In this last region, the dielectric functions have been fitted by the Adachi's critical-point model and the resulting parameters are reported. The optical functions can be applied in the tayloring of the optoelectronic properties and in the optical characterization of multilayer systems based on InGaP.

Concerning the influence of growth parameters, substrate orientation and doping on the optical functions, the following points should be stressed. All the samples, irrespective of the growth temperature and plant, have shown good optical quality and spatial homogeneity. The ordering degree has very little effect on the optical functions from the subgap transparency region up to the restrahlen region. As expected, the order strongly influences the gap E_0 and the E_1 interband peak. The doping has major effects on the FIR and MIR optical functions, while is quite irrelevant in the NIR subgap region; moreover, it modifies the gap through two competitive effects: a gap-shrinkage due to many body interactions and a gap widening due to the structural disorder.

This work has been partially supported by the Agenzia Spaziale Italiana (A.S.I.) – Project "Studio e realizzazione di prototipi di celle solari avanzate a tripla giunzione InGaP/GaAs/Ge per applicazioni spaziali" – and by the Progetto Finalizzato MADESS II –CNR. Authors wish to thank Dr. R. Kudela and Dr. S. Hasenohrl of the IEE of Bratislava for growing the BTS samples, and Dr. C. Bocchi and F. Germini for X-ray investigations.

References

1. M. Razeghi, in *The MOCVD Challenge* (Institute of Physics Publishing, Bristol and Philadelphia, 1995), Vol. 2
2. S. Pellegrino, L. Tarricone, Mat. Chem. Phys. **66**, 189 (2000)
3. M. Razeghi, III-Vs Rev. **10**, 37 (1997)
4. I. Eliaschevick, J. Diaz, H. Yi, L. Wang, M. Razeghi, Appl. Phys. Lett. **66**, 3087 (1995); A. Moto, S. Tanaka, T. Tanabe, S. Takagishi, Solar Energy Mat. Solar Cells **66**, 585 (2001)
5. E. Greeger, P. Rial, M. Moser, T. Kippenberg, P. Kiesel, G.H. Dohler, Appl. Phys. Lett. **71**, 3245 (1997)
6. T. Takamoto, E. Ikeda, H. Kurita, M. Ohmori, Appl. Phys. Lett. **79**, 13 (1997)
7. C.C. Hsu, Y.F. Yang, H.J. Ou, E.S. Yang, H.B. Lo, Appl. Phys. Lett. **71**, 3249 (1997)
8. G.S. Horner, A. Mascarenhas, S. Froyen, R.G. Alonso, K. Bertness, J.M. Olson, Phys. Rev. B **47**, 4041 (1993)
9. A. Gomyo, T. Suzuki, S. Iijima, Phys. Rev. Lett. **60**, 2645 (1988)

10. A clear review of the causes and consequences of spontaneous atomic ordering in semiconductor alloys (particularly InGaP) and a summary of the optical fingerprints measured by many authors can be found by A. Zunger, MRS Bull. **22**, 20 (1997), and references therein
11. P. Ernst, C. Geng, F. Scholz, H. Schweizer, Y. Zhang, A. Mascarenhas, Appl. Phys. Lett. **67**, 2347 (1995)
12. S. Ozaki, S. Adachi, M. Sato, K. Ohtsuka, J. Appl. Phys. **79**, 439 (1996)
13. M. Schubert, V. Gottschalch, C.M. Herzinger, H. Yao, P.G. Snyder, J.A. Woollam, J. Appl. Phys. **77**, 3416 (1995)
14. M. Schubert, J.A. Woollam, G. Leibiger, B. Rheinlander, I. Pietzonka, T. Sab, V. Gottschalch, J. Appl. Phys. **86**, 2025 (1999)
15. H. Lee, D. Biswas, M.V. Klein, H. Morkoc, D.E. Aspnes, B.D. Choe, J. Kim, C.O. Griffiths, J. Appl. Phys. **75**, 5040 (1994)
16. H. Lee, M.V. Klein, J.M. Olson, K.C. Hsieh, Phys. Rev. B **53**, 4015 (1996)
17. S.H. Wei, A. Zunger, Phys. Rev. B **39**, 3279 (1989)
18. H. Tanaka, Y. Kawamura, H. Asahi, J. Appl. Phys. **59**, 985 (1986)
19. M. Moser, R. Winterhoff, C. Geng, I. Queisser, F. Scholz, A. Dornen, Appl. Phys. Lett. **64**, 235 (1994)
20. R. Wirth, A. Moritz, C. Geng, F. Scholz, A. Hangleiter, Phys. Rev. B **55**, 1730 (1997)
21. G. Lukovsky, M.H. Brodsky, M.F. Chen, R.J. Chicotka, A.T. Ward, Phys. Rev. B **4**, 1945 (1971)
22. E. Jahne, W. Pilz, M. Giehler, L. Hildisch, Phys. Stat. Sol. (b) **91**, 155 (1979)
23. F. Alsina, H.M. Cheong, J.D. Webb, A. Mascarenhas, J.F. Geisz, J.M. Olson, Phys. Rev. B **56**, 13126 (1997)
24. P. Ernst, C. Geng, F. Scholz, H. Schweizer, Phys. Stat. Sol. (b), **193**, 213 (1996); Appl. Phys. Lett. **67**, 2347 (1995)
25. M. Longo, A. Parisini, L. Tarricone, L. Toni, R. Kùdela, Mat. Sci. Engin. B **86**, 157 (2001)
26. G. Attolini, C. Bocchi, F. Germini, C. Pelosi, A. Parisini, L. Tarricone, R. Kùdela, S. Hasenohrl, Material Chem. Phys. **66**, 246 (2000)
27. S. Zollner, Appl. Phys. Lett. **63**, 2523 (1993)
28. D.E. Aspnes, A.A. Studna, Phys. Rev. B **27**, 985 (1983)
29. M.J. Gregor, P.G. Blome, R.G. Ulbrich, P. Grossmann, S. Grosse, J. Feldmann, W. Stolz, E.O. Göbel, D.J. Arent, M. Bode, MK.A. Bertness, J.M. Olson, Appl. Phys. Lett. **67**, 3572 (1995)
30. R.P. Schneider, Jr. E.D. Jones, D.M. Follstaedt, Appl. Phys. Lett. **65**, 587 (1994)
31. K.A. Mader, A. Zunger, Appl. Phys. Lett. **64**, 2882 (1994)
32. S. Froyen, A. Zunger, A. Mascarenhas, Appl. Phys. Lett. **68**, 2852 (1996)
33. P. Lautenschlager, P.B. Allen, M. Cardona, Phys. Rev. B **33**, 5501 (1986)
34. L. Francesio, P. Franzosi, M. Caldironi, L. Vitali, M. Dellagiovanna, A. Di Paola, F. Vidimari, S. Pellegrino, Mat. Sci. Eng. B **28**, 219 (1994)
35. *Handbook of optical constants of solids*, edited by E.D. Palik (Academic Press, Orlando, 1985)
36. E. Bedel, R. Carles, G. Landa, J.B. Renucci, Rev. Phys. Appl. **19**, 17 (1984)
37. See for example O.S. Heavens, *Optical properties of thin solid films* (Butterworths Scientific Publications, London, 1968)
38. C.C. Kim, J.W. Garland, H. Abad, M. Raccah, Phys. Rev. B **45**, 11749 (1992)
39. C.C. Kim, J.W. Garland, M. Raccah, Phys. Rev. B **47**, 1876 (1993)
40. S. Adachi, *Optical properties of crystalline and amorphous semiconductors* (Kluwer Academic Publisher, Boston, 1999)